## Abstract:

There is a need to develop tissue engineering based approaches to address the shortage of donor corneas worldwide for transplantation. To do this a novel approach to fabricate three-dimensional hydrogels using free-radical polymerization was investigated to generate constructs for corneal stromal tissue regeneration. Different ratios of silk fibroin (SF) to polyacrylamide (PA) were used to fabricate semi-interpenetrating hydrogels. Scanning electron micrograph displayed the interconnectivity of pores within the fabricated hydrogels. Pore sizes ranged from 25 to 66 µm. Scaffolds with increasing concentration of SF had enhanced β-sheet structure (verified by Fourier transform infrared spectroscopy). The biological response of human corneal stromal cells to these hydrogels was examined using cellular adhesion, proliferation, cytoskeleton organization, gene expression and immunocytochemical analysis. The fabricated hydrogels possess rapid gelation (~3min) at 37 °C, 84% porosity facilitating keratocyte migration during healing, improved cellular adhesion and no cytotoxicity, indicating their efficiency for in-situ corneal tissue regeneration. Presence of SF in semi-interpenetrating network hydrogel enhanced cellular proliferation, elevated GAG deposition, and increased expression of keratocyte genes, normally associated with healthy corneal stromal tissue. This study acts as an initial step towards fabricating SF based semi-interpenetrating network hydrogels for developing clinically applicable ocular implants.

**Declaration of interests**

☒The authors declare that they have no known competing financial interests or personal relationships that could have appeared to influence the work reported in this paper.

☐The authors declare the following financial interests/personal relationships which may be considered as potential competing interests:

**Author statement:**

Bhattacharjee P: Conception and design of study; Acquisition of data; Analysis and interpretation of data; Drafting the manuscript.

Ahearne M: Conception and design of study; Review and editing of manuscript; Acquisition of research funding.

# Silk fibroin based interpenetrating network hydrogel for corneal stromal regeneration

*Promita Bhattacharjee[1,2] and Mark Ahearne[1,2*]*

[1]Trinity Centre for Biomedical Engineering, Trinity Biomedical Sciences Institute, Trinity College Dublin, the University of Dublin, Dublin, Ireland.

[2]Department of Mechanical, Manufacturing and Biomedical Engineering, School of Engineering, Trinity College Dublin, the University of Dublin, Dublin, Ireland.

* Corresponding author (ahearnm@tcd.ie)

## Abstract:

There is a need to develop tissue engineering based approaches to address the shortage of donor corneas worldwide for transplantation. To do this a novel approach to fabricate three-dimensional hydrogels using free-radical polymerization was investigated to generate constructs for corneal stromal tissue regeneration. Different ratios of silk fibroin (SF) to polyacrylamide (PA) were used to fabricate semi-interpenetrating hydrogels. Scanning electron micrograph displayed the interconnectivity of pores within the fabricated hydrogels. Pore sizes ranged from 25 to 66 μm. Scaffolds with increasing concentration of SF had enhanced β-sheet structure (verified by Fourier transform infrared spectroscopy). The biological response of human corneal stromal cells to these hydrogels was examined using cellular adhesion, proliferation, cytoskeleton organization, gene expression and immunocytochemical analysis. The fabricated hydrogels possess rapid gelation (~3min) at 37 °C, 84% porosity facilitating keratocyte migration during healing, improved cellular adhesion and no cytotoxicity, indicating their efficiency for in-situ corneal tissue regeneration. Presence of SF in semi-interpenetrating network hydrogel enhanced cellular proliferation, elevated GAG deposition, and increased expression of keratocyte genes, normally associated with healthy corneal stromal tissue. This study acts as an initial step towards fabricating SF based semi-interpenetrating network hydrogels for developing clinically applicable ocular implants.

**Keywords:** Silk fibroin; Polyacrylamide; Interpenetrating network; Tissue engineering, Cornea.

## 1. Introduction:

Cornea is the outer most, transparent layer of the eye. The major structural and functional unit of the cornea is the stroma. The stroma has a highly ordered, hierarchical organized extracellular matrix (ECM) and quiescent keratocytes[1,2] to maintain corneal transparency. Corneal injury, generally caused by infection or trauma, may lead to wound healing and impaired vision. According to World Health Organization's (WHO) report, corneal scares are the fourth leading cause of blindness worldwide[3]. Presently, corneal transplantation is one of the most acceptable and effective, clinical treatment to restore/improve vision for stromal corneal damage after injury. Large global shortage of corneal donors – only 1.4% of the present demand[3] - restricts such transplants. Keratoplasty is necessary for many cases to assuage the suffering, pain and to regain vision, but in some cases, the recipient may not be able to accept an allograft. To address these issues, researchers have been exploring new methods to obtain corneal tissue using tissue engineering. One of the most challenging tissue to engineer is corneal stroma due to its composition, thickness, complicated highly ordered structure, and need for transparency[4]. So far, most research has focused on using three-dimensional hydrogels [5,6,7,8,9] or decellularized corneal scaffolds[10,11,12].

In situ hydrogel formation is a one of the most attractive choices for soft tissue regeneration (like cornea, skin). It limits risk of infection, lowers invasive surgical complexity, strengthens interaction between tissue and hydrogel and covers up wounds, promptly, without crumple[13]. In situ formed hydrogels show more advantages over pre-formed hydrogel regarding entrapping of bioactive molecules, cells, or drugs with precursor molecules before the formation of gel and efficient delivery at the target site [14]. There do exist some crucial challenges (like rapid gelation at physiologically tolerable temperatures, cross-linking in aqueous environments and tolerance of moisture) associated with fabricating injectable, in situ hydrogels[15].

The most commonly used polymerization procedure involves radical or photo polymerization utilizing photoinitiator. This is not favoured for *in vivo* injection[16]. To address this issue, free radical polymerization, providing homogeneity in the cross-linked network[17], was introduced to fabricate in situ hydrogels system with desired biocompatibility and biodegradability[18]. Natural and synthetic polymers, which have been used extensively to fabricate hydrogel, have certain limitations. Characteristics of natural polymer-based hydrogels vary from batch to batch, whereas biodegradability and biocompatibility is a major problem associated with synthetic polymer-based hydrogels[19]. Faced with this conundrum, the solution would be formulating a co-polymer system, consisting of natural and synthetic polymers – whether blended, cross-linked, or physically entrapped[20,21].

Polyacrylamide (PA) is used as a cell-based, synthetic biomaterial. Pure PA hydrogel are brittle, however, they possess several advantages, making it ideal for creation of in situ hydrogels[22]. These include the ability to modulate the elastic modulus by adjusting the monomer-cross linker ratio; consistent surface chemistry across a range of mechanical

properties; little nonspecific cell-receptor binding; translucent properties and the possibility of fast free-radical polymerization.

Silk fibroin (SF), approved by the U.S. Food and Drug Administration (FDA)[1]for medical use, has established itself as an indispensable biopolymer for tissue engineering applications due to its biocompatibility, controlled biodegradability, production of non-inflammatory by-products, mechanical strength and an ability to stabilize labile compounds[23,24,25]. Furthermore, SF is almost transparent to visible light, an important criteria when choosing biomaterials for ocular constructs [26,27,28,29,30]. The combination of such properties makes SF a promising biomaterial for fabrication of corneal scaffolds.

These aspects of both polymers encourage the exploration of a PA/SF hydrogel construct. If, in such a system, SF could be physically entrapped within the void space of the highly cross-linked PA network without the involvement of any chemical crosslinker, that would open up new opportunities for tissue engineering cornea. The present work reports on the formulation of SF hydrogel through the physical entrapment of SF within the 3D hydrophilic network of PA. Previously, SF based interpenetrating network hydrogel has been investigated for hydrophobic drug delivery[31], controlled release of drugs[32] and wound dressing[33]. A recent study reported that silk fibroin based interpenetrating network hydrogels exhibited high strength and toughness. These properties indicated the potential for future use as biological material[34].To the best of our knowledge, this formulation method to develop SF based 3D interpenetrating network hydrogel for corneal stromal regeneration has not previously been examined. Further, the role of protein concentration on the resultant biomaterial's stability, mechanical flexibility, cytotoxicity and cellular responses with corneal stromal cells was also evaluated.

## 2. Materials and methods:

All reagents and chemicals were procured from Sigma-Aldrich, unless specified otherwise.

### *2.1. Isolation of silk fibroin from Bombyx mori cocoon:*

Silk fibroin (SF) was extracted from Bombyx mori cocoons (Treenway silks, USA) using previously described standard protocol[26]. The SF concentration was adjusted, using 10% (w/v) Polyethyleneglycol (PEG, 10,000 MW) solution, to 4%, 6% and 8% (wt/wt). These concentrations were used throughout this study. The final concentration of protein solution was measured by gravimetric analysis.

### *2.2. Fabrication of composite hydrogels:*

A free radical polymerization using N, N´-methylene bisacrylamide (N,N´-MBAAm) as cross-linker, ammonium persulfate (APS) as free-radical initiator and N,N,N´,N´ tetramethylenediamine (TEMED) as catalyst, was utilized to obtain the semi-interpenetrating network of SF and PA. 30 wt% aqueous PA solution containing 0.5 wt% N, N´-MBAAm, 5 wt% of APS and 0.5 wt% of TEMED was mixed with equal volumes of SF solutions of the three

different concentrations to achieve required blended ratios. The PA concentration in the fabricated hydrogel was 15 wt% while SF concentration was varied from 4 to 8 wt% in PA/SF4, PA/SF6 and PA/SF8 respectively. Pure PA hydrogels of 15 wt% served as control, designated as PA. The hydrogels were removed from the moulds after polymerization and washed thrice with de-ionized water to remove of sol fraction. The hydrogels were frozen at -20 °C and lyophilized following the previously established protocol[21]. After lyophilization, hydrogels were treated with absolute ethanol for 5 min and 70% ethanol for 20 min to form a β-sheet structure, before conducting further studies.

### *2.3. Measurement of gelation kinetics:*

As the gelation progressed, viscoelasticity of the precursor solutions increased continuously until the complete network structure was achieved. The gelation time was defined as the duration of time needed to form gel following the incorporation of APS and TEMED. Gelation time was determined according to the time taken by the reactant mixture to turn into a viscous solution and the viscous solution no longer tumbled in the leaned tube position[35].

### *2.4. Evaluation of rheology:*

Rheological analysis were conducted using a MCR 102 rheometer (Anton Paar, Austria) assembled with temperature controlling systems, using a 25 mm diameter parallel plate[11]. Viscosity of precursor solutions was quantified by performing a frequency sweep, from 0.1 to 1000 Hz, at 5% strain at, 15 °C.

### *2.5. Morphology and porosity measurement:*

The hydrogels microstructure was analysed using scanning electron microscopy (SEM, SUPRA 35 VP, Carl Zeiss). Following fabrication, the hydrogels were washed thrice with de-ionized water to take off unreacted monomers. The fabricated hydrogels were then cryo-fractured by dipping in liquid nitrogen (-196 °C) and lyophilized. The completely dried resultant hydrogels were used to conduct SEM analysis after gold-coating, using a sputter coater. The pore sizes of hydrogels were measured using ImageJ software (average of 30 randomly selected pores). Physical images of hydrogels have also been presented.

### *2.6. Porosity measurement:*

A solvent replacement method was utilized to measure the porosity of the hydrogels[21]. Disc shaped hydrogels (6 mm diameter, 6 mm height) were prepared for this study and total volume of hydrogel (v) was determined from its dimensions. Completely dried hydrogels were submerged in known volume ($v_1$) of hexane at room temperature for 5 min. The hydrogels were then taken out and the volume of unabsorbed hexane ($v_2$) was measured.

### *2.7. Transparency:*

The transparency and macroscopic image of fabricated hydrogels was evaluated. To measure the light transmission, hydrogels were placed in a 12-well plate, after soaking in phosphate buffer saline (PBS), at 37 °C, for 2 days. PBS was used as a blank control. A microplate reader

(Synergy HTX, BioTek) was used to determine the light transmittance for wavelengths between 400 nm and 750 nm. An average of three measurements of each composition, under each wavelength measured was considered.

### *2.8. Chemical and thermal characterization:*

To analyse the chemical composition of the hydrogels, attenuated total reflectance-Fourier transform infrared (ATR-FTIR, Nexus-870, Thermo Nicolet Corporation, USA), over a wave number range of 2500–500 $cm^{-1}$ under ambient conditions was conducted. Thermogravimetric Analysis (TGA) was performed (Perkin Elmer Pyris Diamond TG-DTA thermo-gravimetric analyser) from 50°C to 300°C, at a rate of 10 °C /min, under synthetic air ($N_2$–$O_2$ is 80:20).

### *2.9. Stability of PA/SF hydrogels:*

The stability of the PA/SF hydrogels was evaluated to quantify the release of SF over time from the composite constructs. The hydrogels were incubated in given volumes of PBS (pH 7.4) at 37 °C. To avoid fungal contamination, 0.02 wt% sodium azide was added to PBS. At specified time-points, PBS extracts were collected and measured for protein concentration with Bradford assay method. The protein released in PBS was quantified from the standard curve from its corresponding OD value at 595 nm.

### *2.10. Evaluation of percentage equilibrium water content (EWC) and sol fraction:*

Gravimetric analysis yielded the percentage of equilibrium water content of each composition [36]. The fully dried hydrogels were incubated in three different sets of PBS with pH 3, 7.4 and 11 respectively at 37°C for 48 h to equilibrate. After removing excess water from the surface, the swollen constructs were weighted immediately, and the percentage equilibrium water content was quantified as a ratio of weights of equilibrium swollen gel to dried gel.

The remaining sol fractions after gelation was measured for all hydrogels utilizing a standard protocol with minor modification[36]. Dry weight of each lyophilized hydrogels was noted down, and the dried hydrogels were incubated in de-ionized water at 37°C for 24 h. The swollen hydrogels were removed after incubation, wiped properly and dried again. After re-drying, the final weight was measured. The percentage sol fraction was determined as a ratio of weight loss after re-drying to initial dry weight.

### *2.11. Evaluation of swelling ratio:*

Conventional gravimetric analysis was performed to determine the swelling behaviour of the hydrogels[21]. Lyophilized hydrogels were incubated in deionized water at 37°C. After incubating for a pre-determined time interval, samples were removed, blotted to dry and weighed. The swollen gels were further lyophilized and re-weighed. The mass swelling ratio was quantified from the ratio of wet weight and dry weight.

### *2.12. In vitro enzymatic degradation:*

The in vitro biodegradation of the fabricated hydrogels was evaluated in Protease XIV (from Streptomyces griseus, 1.0 mg/ml) and phosphate buffer solution (PBS, pH 7.4) at 37 °C, for 28 days[37]. After formulation, three samples of each composition were weighed and lyophilized. The weight after lyophilization of each hydrogel was noted to determine the percentage monomer for each composition. The known weight, disk shaped hydrogels were immersed in 10 ml enzyme and PBS (pH 7.4) solution, with 0.02 wt% sodium azide added to prevent bacterial contamination. The enzyme solution was changed every alternate day. At pre-determined time interval, 3 samples of each composition were removed and lyophilized. The weight of the lyophilized samples was determined and correlated to initial dry weight (initial weight of each hydrogel × % macromer) to determine the percentage mass loss with time. The results were presented as the percentage mass remaining over time.

*2.13. Cell isolation and culture:*

Isolation of human corneal stromal cells from donor tissue were performed as per previously described protocol[38], in accordance with the Declaration of Helsinki. After physically discarding the epithelium and endothelium of the corneas, the remaining stromal tissue was cut into tiny pieces and immersed in culture media consisting of Dulbecco's Low Glucose Modified Eagles Medium (DMEM) (Hyclone; Thermo Fisher Scientific) and supplemented with 10% fetal calf serum (Hyclone) and 1% penicillin/streptomycin onto a culture plate. When cells had migrated out from the stromal tissue and attained confluency of around 80–90%, they were trypsinized, centrifuged and counted using a hemocytometer after suspending them in the medium. The cells were then cultured to evaluate the biocompatibility of fabricated hydrogel in standard culture flasks in a controlled, humidified environment of 5% $CO_2$, at 37 °C. Cells at passage 2 were utilized in the current study.

The hydrogels (4 mm diameter × 2 mm thick) were sterilized by treating with 70% ethanol followed by a 30 min exposure to UV. Hydrogels were then washed thrice using sterile PBS (pH 7.4) for 30 min and immersed in culture medium for 6 h to assure that the hydrogels would maintain a favourable environment to the seeded cells. The hydrogels were partially dried before couple of hours of cell seeding to allow better cell penetration. Each hydrogel was seeded with 100 µl of cell suspension in media containing $0.5\times10^5$ cells. For 1 h after seeding, cell-hydrogel constructs were maintained at 37 °C and 5% $CO_2$, in a humidified environment, to boost cell adhesion. Cell seeded hydrogels were cultured in serum free media containing of DMEM/F12 (Hyclone; Thermo Fisher Scientific), supplemented with 1% penicillin/streptomycin, 100 µg/ml L-ascorbic acid and 1 µl/ml Insulin-Transferrin-Selenium (100×, Gibco) medium for up to 21 days. Cell culture media was replaced every alternate day.

*2.14. Cellular adhesion and toxicity assay:*

After 1, 3 and 5 h of cell seeding, cell adhesion onto hydrogels was performed as per previously established protocol[39]. Briefly, without interrupting the cell laden constructs, culture media was flushed gently onto the culture plate to detach any cells that might have

been loosely attached to the culture plate. The concentration of unattached cells was then counted using hemocytometer, treating the chamber with 10µl of this cell suspension. The number of adhered cells to the hydrogels was determined by subtracting the density of unattached cells from the cell seeding density. Following the manufacturer's protocols, cell metabolic activity was performed at pre-determined time intervals using a PrestoBlue assay (Molecular Probes; Invitrogen, Carlsbad, CA), over 21 days of culture period.

*2.15. In vitro biocompatibility and cytoskeletal organization:*

After 5 days of culture, cell laden hydrogels were conducted for live/dead assay (Molecular Probes, USA), where live cells were stained by calcein (green coloration; excitation: 488 nm) and dead cells by ethidiumhomodimer (red coloration; excitation: 543 nm). The stained hydrogels were investigated through confocal microscopy (Leica SP8, Leica).

Cytoskeletal organization of cell laden hydrogels were examined after 10 days of culture. After fixing the constructs using 4% paraformaldehyde for 15 minutes at room temperature (RT), the fixed constructs were permeated with 0.1% Triton X-100 for 5 min, blocked with 1% bovine serum albumin (BSA) for 1h. and stained with phalloidin-TRITC. The constructs were counterstained with 4',6-diamidino-2-phenylindole (DAPI). The Leica SP8 confocal microscope was utilized for imaging, followed by image post-processing using LAS X Advanced software.

*2.16. Immunofluorescent staining:*

After 14 days of culture, cell laden hydrogels were pre-processed for immunocytochemistry analysis. After permeabilization and blocking, constructs were incubated with primary antibodies, overnight, at 4°C. The following primary antibodies were employed: ALDH3A1, CD34, and α-SMA. Following incubation, three, 5-min washes with 1% BSA in PBS were carried out to get rid of the unbound antibody. The cell laden hydrogels were then incubated with secondary antibody for 1 h at room temperature followed by washing three times for 5 min with 1% BSA in PBS. Constructs were then treated with DAPI to counterstain the nuclei. Only secondary antibody staining was done as negative control. Laser scanning confocal microscopy (Leica SP8) was used to image stained cell laden hydrogels. Details of antibodies and the immunofluorescent staining protocol are previously reported [12].

*2.17. Gene expression by real-time Real Time-PCR:*

Real-time reverse transcription PCR was performed to assess relative gene expression after 14 days of culture following previously established protocol[39]. The following primers (Applied Biosystems, Biosciences, Dublin, Ireland) were procured and examined: ALDH3A1 (Hs00964880_m1), collagen type III (COL3A1; Hs00943809_m1), collagen type I (COL1A1; Hs00164004_m1), collagen type V (COL5A1; Hs00609133_m1), decorin (DCN; Hs00754870_s1), glyceraldehyde-3- phosphate dehydrogenase (GAPDH; Hs02758991_g1), keratocan (KERA; Hs00559942_m1), and lumican (LUM; Hs00929860_m1). Based on the ΔΔCt methodology, gene expressions were normalized against reference gene, GAPDH. The gene expression values were then determined and presented in an exponential form, $2^{-\Delta\Delta Ct}$.

### *2.18. Biochemical assays:*

Following previously described protocol**,** biochemical analysis of sulfated glycosaminoglycans (sGAG) and DNA was evaluated after 14 and 28 days of culture periods[39]. Cells in the hydrogels were macerated utilizing a digestion solution (125 µg/ml papain, 5 mM L-cysteine, 100 mM Na2HPO4, 5 mM EDTA, pH 6.8) for 16 h, at 60 °C. A dimethylmethylene blue (DMMB) binding assay (Blyscan; Biocolor Ltd., Antrim, UK) was performed to measure sGAG. After mixing each sample with the DMMB solution, the absorbance was evaluated at 590 nm wavelength. Using a standard plot of bovine chondroitin sulfate, total sGAG of each sample was deduced and a Bisbenzimide Hoechst 33258 DNA assay was performed to normalize data to DNA.

### *2.19. Statistical analysis:*

One-way ANOVA was performed, followed by Tukey's post-hoc HSD test. Significant differences are presented as ***$p < 0.001$; **$p < 0.01$; *$p < 0.05$. Data presented uses the format of mean ± standard deviation (SD). Sample size, unless otherwise specified, is 3.

## 3. Results:

### *3.1. Fabrication of hydrogel network*

The free radical polymerization reaction in an aqueous medium was used to fabricate PA/SF semi-interpenetrating hydrophilic networks at room temperature. The hydrogels promptly took the shape of moulds used for formulations. The possible mechanism of crosslinking has been presented in Figure 1. Due to different non-covalent bonds (including hydrogen bonding), as well as electrostatic interactions, PA formed a reversible complex in aqueous solution[40]. In the presence of aqueous SF solution, the polymerization of acrylamide moderately induced the formulation of semi-interpenetrating network hydrogels[41]. Polymerization of PA and SF initiates and as a consequence, a semi-interpenetrating network is developed by the cross linking of the liner polymer in the immediate presence of another[41]. APS and TEMED were used as combination of redox initiators in the current reaction system. TEMED accelerated the reaction, and the free radicals were formed due to the dissociation of APS. These free radicals should not be present in the resultant hydrogels as a result of their short lifetime[42]. Both, covalent and ionic bonds were present in the fabricated hydrogels. The 3D framework and rigidity of the hydrogels was supported by the covalent bonds, whilst higher mechanical strength and pH sensitivity was significantly influenced by ionic bonds[43]. Hydrogels with varying SF concentrations ranging from 4 to 8 wt% were fabricated and designated as PA/SF4, PA/SF6 and PA/SF8, corresponding to final SF concentration in the hydrophilic network as 4, 6 and 8 wt%. The pure PA gels (15 wt%) served as control and were designated as PA.

### *3.2. Physical characterization of hydrogels:*

The protein concentration significantly affected the gelation rate of semi-interpenetrating hydrogels (Fig. 2(a)) with the increasing SF concentration leading to longer gelation times.

This was due to the higher concentration of protein being entangled within rigid polymeric network due to physical interaction. The gelation times of the hydrogels in this study ranged from 2 to 3.5 min. The fastest gelation was recorded by PA/SF4 (~2.2 min.), followed by PA/SF6 and PA/SF8 respectively. Due to the rapid gelation, gelation kinetics of PA could not be accurately quantified. The viscosity was measured by increasing shear rates at 15 °C. Regardless of protein concentration, shear thinning characteristics were noticed in all precursor solutions (Fig. 2(b)).

The fabricated hydrogels are required to have optical properties similar to a healthy cornea. Quantitatively, the percentage of visible light transmittance through the hydrogels was between 80% and 95% (Fig. 2(c)). The transmittance decreased as the light wavelength entered the UV region.

After fabrication, hydrogels were cryo-fractured vertically to examine the native structure of hydrogels (Fig. 2(d)). An uninterrupted homogeneous interconnected porous morphology within fabricated hydrogels was revealed through SEM analysis. The internal morphology (pore size and structure) was dependent on various factors like lyophilization process, crosslinking density as well as concentration of SF and PA. The overall pore size was 20-75 µm, with mean pore sizes of 66±9 µm, 52±7 µm, and 32±4 µm for PA/SF4, PA/SF6, and PA/SF8 respectively. The pure polyacrylamide gel exhibited the smallest mean pore size of 25±3 µm. In the blended hydrogels, pore sizes reduced with increased protein concentration (refer Table I).

### *3.3. Chemical characterization by FTIR spectroscopy:*

The interaction of SF and PA within the semi-interpenetrating network was investigated by analysing the positions of the peaks of amide I, amide II, and amide III in infrared spectrum. Fig. 3(a) represents IR spectrum of SF (magnified peaks were presented inset), PA, and PA/SF composite hydrogels. Of the major vibration peaks detected, the following three vibration peaks associated with SF were identified: 1650–1630 $cm^{-1}$ for amide I (C=O stretching), 1540–1520 $cm^{-1}$ for amide-II (secondary NH bending, due to β-sheet structure), and 1270–1230 cm−1 for amide III (C-N and N-H functionalities)[39]. Absorption peaks at ~1535 cm−1 and ~1648 cm−1 corresponded to the β-sheet structure (amide II). Protein conformation was confirmed from the presence of an amide I band, embodied by the C=O stretching vibration[44]. Hydrogen bond strength, for those between N-H and C=O groups, impacts the vibration frequency of the band. Protein backbone conformational structure controls bond strength[44]. Crosslinking of SF and PA exhibited peak shift of the composite hydrogels. All the hybrid hydrogels had the characteristic peaks of polyacrylamide, including the peak at 1682 cm-1, corresponding to the C=O of the amide group, the peak at 1450 cm-1 corresponding to C-N (amide III stretching) and the peak at 1120 $cm^{-1}$ [C-N and N-H bonds (amide III)]. Moreover, all composite hydrogels represented all the corresponding peaks of SF and PA without major alteration and peak shift, except for amide II at 1534 cm-1. Generally, amide II reflects the change in hydrogen bond environment[21]. The addition of SF into the PA network affected the hydrogen bond mediated amide-amide interactions. The interpenetration reduced the unordered nature of SF which

supported the findings of enhanced mechanical properties of the hydrogels. This result indicates crosslinking of SF and PA, without any major structural alteration and implies structural stability of the hydrogels.

### *3.4. Thermal analysis by TGA:*

To investigate the thermal stability of the hydrogels, thermal gravimetric analysis was performed (Fig. 3(b)). Hydrogels showed single step decomposition behaviour. A mass change was clearly noticed over a temperature range of 95-100 °C due to the immense loss of adsorbed water. Hydrogels experienced moderate decomposition above 100 °C. The complete thermal decomposition (0% w/w residue) of polyacrylamide occurred at ~198°C. This may happen due to the loss of ammonia with the formation of imide group via cyclisation[45]. The decomposition temperature of hydrogels was ~186° C, ~172° C and ~163° C for PA/SF4, PA/SF6, and PA/SF8 respectively. The decomposition temperature (onset) points decreased with increase of SF concentration.

### *3.5. Stability of SF interpenetration within the hydrogels:*

Three-dimensional semi-interpenetrating network of hydrogels are capable of entrapping a large amount of protein (~85%) after 21 days. A burst release of protein was observed within the 96 h after fabrication of hydrogels. Thereafter, a sustained and stable release profile was recorded. The total fraction of SF released was approximately 7.5, 11 and 14.8% for PA/SF4, PA/SF6, and PA/SF8 respectively (Fig. 3(c)) ($p < 0.05$). Integration of SF protein within the cross-linked network of PA gel was stable.

### *3.6. Swelling characteristics of the hydrogels:*

The swelling characteristics of the hydrogels was clearly visible. The swelling ratio, corresponding to water absorption, substantially increased with SF protein concentration due to the consequence of an interaction (Fig. 4(a)). The equilibrium water content of lyophilized hydrogels under different pH (pH 3, 7.4 and 11) of PBS has been presented in Fig. 4(b). A linear shift in equilibrium water content was recorded with increased pH. There was no significant difference in equilibrium water content observed among different compositions. The average equilibrium water content of the hydrogels was 61% in a pH 3 medium. It increased to 80% ($p < 0.05$) and 92% ($p < 0.01$) in pH 7.4 and pH 11 mediums, respectively. Sol fraction (%) of fabricated hybrid semi-interpenetrating structural hydrogels at 37 °C has been reported at Table I.

### *3.7. In vitro degradation:*

The degradation of all the hydrogels in PBS (pH 7.4) at 37° C (Fig. 4(c)) and in Protease XIV (Fig. 4(d)) was evaluated and has been presented as %weight remaining after 28 days. The percentage of SF significantly affected the mass loss. At day 28 in PBS, the mass left for PA, PA/SF4, PA/SF6, and PA/SF8 were 88%, 84%, 81% and 75% respectively. Treatment with the enzyme over 28 days showed a time dependent decrease in dry weight. At day 28 in enzyme,

the mass left for PA, PA/SF4, PA/SF6, and PA/SF8 were 74%, 64%, 56% and 48% respectively. Controlled biodegradation is an essential feature for scaffolding materials as it can regulate cell viability, growth and host response[46].

The rate of in vivo degradation of the scaffolding material should ideally correspond with the rate of new tissue formation. There are similarities between degradation of silk-based matrix through Protease XIV and the degradation produced by some typical human enzymes[47].

### *3.8. Cell adhesion and proliferation:*

The adhesion of the corneal stromal cells to the surface of composite hydrogels after 5h culture was evaluated (Fig. 5(a)). Within the first hour, approximately ~55%, ~78%, ~84% and ~82% of cells had attached to PA, PA/SF4, PA/SF6, and PA/SF8 hydrogels respectively. All composite hydrogels showed significantly higher ($p < 0.05$) cellular adhesion compared with control (PA). There was no significant difference in cellular adhesion between different composite hydrogels 5 h after seeding. Cells that attached efficiently upon hydrogels are further expected to form a well-ordered organized ECM[39] that is essential for successful tissue regeneration.

The cells proliferated and spread out within the hydrogels over the period of culture. Proliferation was investigated at day 3, 7, 14 and 21 (Fig. 5(b)). No significant difference in terms of cellular proliferation for short-term culture period (day 3) was recorded between different composite hydrogels and the control. This result indicates the non-cytotoxicity of material as hydrogel did not have any detrimental effect on cell growth. The cellular proliferation was significantly increased with time in all cell-laden constructs. Cell metabolism was significantly higher ($p < 0.01$) for all composite hydrogels when compared with control after 21 days of culture. However, a slow rate of cellular proliferation for all compositions was recorded over the whole culture period, probably due to the use of low glucose, serum-free media. Human corneal stromal cells can survive for a long period of time in culture when maintained in low glucose condition as well as retaining keratocyte-characteristic phenotype in serum-free environment[48].

### *3.9. Cell viability and cytoskeletal organization:*

The viability of cells on different hydrogels was evaluated using a live/dead staining assay (Fig. 5(c)). Only viable cells (in green) and no dead cells (red) were observed on all hydrogels, indicating non-cytotoxicity of the hydrogels. There appears to be more viable cells present on PA/SF6 and PA/SF8 hydrogels, followed by PA/SF4 and PA hydrogels. This would seem to associate with the findings from the proliferation assay and imply that hybrid hydrogels are highly efficient at supporting cell proliferation.

The cytoskeleton organization of cells exhibits a crucial function in regulating cell adhesion, migration and contractibility of matrix. More well distributed and stressed actin fibres were present in cells on all composite hydrogels compared to control (PA) (Fig. 5(d)). Less number of cells were observed on control hydrogel (PA) when compared with composite hydrogels.

Actin distribution was irregular and sparse as well as being restricted to the immediate environs of the cell in the control samples.

### *3.10. Gene expression:*

Gene expression of several keratocyte markers was evaluated using rtPCR after 14 days of culture. Hybrid hydrogels significantly increased the expression of ALDH3A1, keratocan, decorin and lumican by day 14 (Fig. 6(a)). ALDH3A1 expression was significantly increased for PA/SF4, PA/SF6, and PA/SF8 (~9.6 ± 1.2, ~11.9 ± 0.89 and ~11.3 ± 1.1–fold increase, respectively) when compared to PA at day 14 (~4.7 ± 0.7–fold increase). A significant increase in keratocan was demonstrated for PA/SF4, PA/SF6, and PA/SF8 (~6.2 ± 1.3, 7.5 ± 1.2 and 7.81 ± 1.4–fold increase, respectively) compared to PA (2.8 ± 0.5–fold increase).Significant increments for decorin and lumican were also recorded for all hybrid hydrogels, compared to control. Expression of collagen type I, III and V, the most abundant collagens in the corneal stroma, were also assessed (Fig. 6(a)). Collagen type I, type III and type V expression was significantly enhanced by day 14 for PA/SF4 (~7.8,~8.9 and ~5.2 -fold increase, respectively), PA/SF6 (~8.4, ~11.5 and~7 -fold increase, respectively) and PA/SF8 (~8.3,~11.6 and ~7.4 -fold increase, respectively) compared to ~3.7,~4.3 and ~2–fold increase in the PA hydrogel. The increased expression of these proteins should lead to improved matrix deposition, which is vital for tissue formation.

### *3.11. Characterization of ECM:*

Cells are required to synthesize and secrete corneal specific ECM to develop corneal tissue. The most common, negatively charged macromolecules, present in corneal stromal ECM, are the glycosaminoglycan (GAG) polysaccharides. Quantification of GAG synthesis for cells on PA/SF4 (~3.67 µg), PA/SF6 (~5.03 µg) and PA/SF8 (~4.82 µg) matrices demonstrated that significantly more GAG was present when compared to PA (~2.11 µg) at day 14 (Fig. 6(b)). A similar trend was present when the GAG was normalized to the DNA present at day 7 and 14 (Fig. 6(b)).

### *3.12. Immunocytochemistry:*

Cell laden hydrogels were further analysed through immunohistochemistry (Fig. 7). Immunocytostaining confirmed the results from rtPCR with cell-laden hydrogels staining positive for ALDH3A1 whereas α-SMA remained negative. Expression of CD34, a hematopoietic stem cell marker and an adhesion molecule, was also investigated for all fabricated hydrogels. Positive staining of CD34 signifies that hydrogels may have a positive function in keeping the keratocytes attached in their micro-niche, between the collagen lamellae[49]. However, the myofibroblastic differentiation was limited on all hybrid hydrogels.

## 4. Discussions:

We have demonstrated that interpenetrating network hydrogels based on SF and PA have the potential to be used for in-situ repair and regeneration of damaged cornea. The fast gelation speed of the hydrogels enables them to be injected into the repair site where they can form a stable hydrogel. The gelation time in the current study is easily controlled by varying the protein concentration. SF shows great promise as a material to fabricate scaffolds to repair tissue as it can easily simulate many advantageous properties of natural ECM and bolster cellular migration, viability and organization[23]. The free-radical polymerization reaction at a close to physiological pH in an aqueous system was used to formulate three different PA/SF composite hydrogels. The concentration of SF had a controlling effect on gelation time. We report gelation times between 2.2 and 3.5 min and increasing SF concentration would further prolong the gelation. A gelation time of less than 3 min is required for in situ sealants[50].

A compact-tighten network with smaller diameter of pores was developed within the composite hydrogels when we used higher concentration of SF. Samples with higher protein concentration hold less water. Any water molecules in an SF solution would exist dispersed within an interconnected network but when immersed in liquid nitrogen, they would rapidly turn into ice crystals[51]. Upon lyophilization of the once frozen constructs, the crystals tend to sublimate, leaving pores in their place. Smaller pores would also be subjected to greater forces of surface tension[52]. This could justify why the pore walls appear to thicken with increasing in SF concentration. Mechanism of pore formation was textured by the lyophilization process [53]. The process comprises three stages: freezing, primary drying and secondary drying. Cooling runs under atmospheric pressure at a constant rate from 15 ˚C to – 20 ˚C followed by a phase at constant temperature of - 20 °C during 90 min. Primary drying occurs at low pressure 187 (0.010 mbar) and - 20 °C for 12 h and secondary drying at 30 °C for 2 h. The freezing temperature before lyophilization was shown to have an impact on the characteristics of the resulting hydrogel. In particular, samples that were frozen at – 20 ˚C and – 80 ˚C resulted in open pore structures after lyophilization, whereas parallel sheet structure was obtained at – 196 ˚C [54].

Materials properties such as pore structure, pore size and mechanical properties were also significantly influenced by protein concentration. No phase separation was noticed in the micrographs, implying homogeneous entanglement of SF within the PA network. It has been suggested that pore size ≥ 5 µm is desirable for neo-vascularization[55]. Therefore, ingrowth of keratocytes within fabricated hydrogel would be aided by the pore size of the fabricated hydrogels. Another important property of hydrogels that needs thorough investigation is swelling behaviour. The diffusion properties are substantially influenced by the amount of water absorbed within the hydrogel. The swelling ratio of the fabricated hydrogels was directly proportional to the concentration of SF. This is likely due to the structure of SF. Though fibroin consists of mainly hydrophobic amino acids (e.g., glycine, alanine) and serine, its overall structure is hydrophilic enough to elevate the swelling ratios of the composite constructs[56]. This increased hydrophilicity improves swelling behaviours and enzyme receptiveness. The higher water absorbance of composite hydrogels may be associated with

an increase in the number of hydrophilic groups (-$NH_2$/-CO) as fibroin concentration (wt%) increased. The resultant hydrophilic network assists to form neo-tissue constructs by improving the permeability of oxygen, nutrients and water-soluble metabolites. The flexible 3D network construct which exhibits high water absorbance capability extended the equilibration duration of hydrogels in de-ionized water [57]. Within the network, amide groups (-$NH_2$) hydrolysing into carboxyl groups (-COOH) increased the within-network osmotic pressure, also potentially contributing to swelling[58]. Carboxyl groups dissociate faster in alkaline environments than in acidic environments. Consequently, the composite hydrogels in an alkaline solution had a higher fraction of equilibrium water content than in acidic solution. At the same time, low to negligible electro-repulsive forces in poly-ions in an acidic region would also mean higher affinity between the polymer chains. Hydrogen bonds formed between the carboxyl groups of different polymer improved rigidity and stability of the 3D polymeric network of hydrogels created[58]. Hydrogen bond strength is pH dependent and reduces in alkaline pH. This decrease in hydrogen bonding strength in alkaline medium also loosened the network, increasing water diffusion. This, in turn, exposed more of the hydrophilic SF to water molecules, increasing swelling and enhancing degradation. The degradation of only PA hydrogel may be due to a significant increase in mobility of the molecule in the environment due to the more hydrophilic nature of polyacrylamide with increased content of carboxylic groups after hydrolysis and degradation under various environmental conditions[59,60] .

Weight loss measured during the degradation analysis corresponded to the loss of protein mass. The tangled polyacrylamide chains gradually become less rigid at physiological pH (7.4). The more flexible chains in turn lead to more protein-polymer interaction and changes the structure and distribution of the pores. These changes to the structure and distribution could explain the variation in degradation behaviour of the constructs made from different blend ratios. Hydrogel microstructure is known to contribute significantly to its mechanical properties[61]. The hydrogels containing higher SF fraction had smaller pores. The blended hydrogels were more porous and their pore-walls were thicker, which should make them more resistant to mechanical cracks [61], making them less brittle.

In our study, corneal stromal cells attached promptly to the composite hydrogels and were shown to undergo proliferation. They appeared to mimic their native phenotype and morphology and displayed well organized stressed actin filaments within the composite hydrogels. These findings go towards the biocompatible and cell supportive nature of the fabricated hydrogels. Gene expressions associates with a native keratocyte phenotype were also elevated for the composite hydrogels. Corneal stromal ECM is primarily made of collagens with collagen types I, III and V being predominant. Collagen type I is the most abundant collagen in the stroma and it is present mainly in the fibrils. Hetero polymeric fibril form from interactions between collagens I and V and these interactions also contribute to controlling the fibril diameters[62]. Collagen III, though also present in healthy cornea, its expression in keratocytes has been shown to be upregulated subsequent to an injury[63]. For

the composite hydrogels, we noted an increase in corneal ECM associated gene expression, i.e., for COL I, III and V. This implies the composite constructs activated keratocytes – partly to boost wound healing while also expressing markers related to a quiescent keratocyte. Well-ordered, organized stromal ECM and intracellular crystallines present in the keratocytes are mainly responsible for corneal transparency[64]. One of the highly distinguished crystalline protein that is expressed by keratocytes is ALDH3A1. The upregulated expression of ALDH3A1 was also recorded by cells on composite cell-scaffold hydrogels in the present investigation.

Investigating the intrinsic characteristics and biological relevance of synthetic-natural co-polymeric hydrogels can help us to better understand their formulation mechanism and potential applications. We employed a simple, practically feasible, and economic fabrication method. Our approach does not necessitate any harsh, extraneous cross-linking agents. This leads us to believe that these composite hydrogels would have immense promise in corneal tissue regeneration and therapeutic delivery. Further consideration regarding optimization and investigation of the system with growth factors/drugs/bioactive molecules can be undertaken to improve cellular migration and retention of their inherent phenotype.

## 5. Conclusion:

In the current study, the feasibility of developing a corneal stromal substitute using a modest, economical and rapid fabrication technique was explored. The crucial characteristics of the composite hydrogels, such as gelation time, hydrogel micro-architecture, swelling, equilibrium water content and degradation were affected by SF content. The formulation of SF 3D matrix, without resorting to use of glutaraldehyde or genipin is a major accomplishment. These semi-interpenetrating networks exhibit the favourable properties desired for corneal stromal regeneration with good cell viability, optical properties, and cell phenotype. SF of 6 and 8 wt% concentration accelerated cell adhesion with optimal adsorption and thermal stability which are advantageous for corneal regeneration therapeutics.

## Acknowledgements:

The research is supported by funding from the European Research Council (ERC) under the European Union's Horizon 2020 research and innovation program (grant agreement no. 637460) and from Science Foundation Ireland (15/ERC/3269).

## References:

[1] Zhang, Wei, Jialin Chen, Mingli Qu, Ludvig J. Backman, Aini Zhang, Haoyang Liu, Xiaoping Zhang, Qingjun Zhou, and Patrik Danielson. "Sustained Release of TPCA-1 from Silk Fibroin

Hydrogels Preserves Keratocyte Phenotype and Promotes Corneal Regeneration by Inhibiting Interleukin-1β Signaling." *Advanced Healthcare Materials* 9, no. 17 (2020): 2000591.

[2] Kumar, Pramod, Abhay Pandit, and Dimitrios I. Zeugolis. "Progress in Corneal Stromal Repair: From Tissue Grafts and Biomaterials to Modular Supramolecular Tissue-Like Assemblies." *Advanced Materials* 28, no. 27 (2016): 5381-5399.

[3] World Health Organization, Priority eye diseases, https://www.who.int/blindness/causes/priority/en/index8.html (accessed February 2020).

[4] Ahearne, Mark, Julia Fernández-Pérez, Sophia Masterton, Peter W. Madden, and Promita Bhattacharjee. "Designing Scaffolds for Corneal Regeneration." *Advanced Functional Materials* (2020): 1908996.

[5] Ozcelik, Berkay, Karl D. Brown, Anton Blencowe, Mark Daniell, Geoff W. Stevens, and Greg G. Qiao. "Ultrathin chitosan–poly (ethylene glycol) hydrogel films for corneal tissue engineering." *Acta biomaterialia* 9, no. 5 (2013): 6594-6605.

[6] Rafat, Mehrdad, Fengfu Li, Per Fagerholm, Neil S. Lagali, Mitchell A. Watsky, Rejean Munger, Takeshi Matsuura, and May Griffith. "PEG-stabilized carbodiimide crosslinked collagen–chitosan hydrogels for corneal tissue engineering." *Biomaterials* 29, no. 29 (2008): 3960-3972.

[7] Mimura, Tatsuya, Shiro Amano, Seiichi Yokoo, Saiko Uchida, Satoru Yamagami, Tomohiko Usui, Yu Kimura, and Yasuhiko Tabata. "Tissue engineering of corneal stroma with rabbit fibroblast precursors and gelatin hydrogels." *Molecular vision* 14 (2008): 1819.

[8] Ahn, Jae-Il, Lucia Kuffova, Kimberley Merrett, Debbie Mitra, John V. Forrester, Fengfu Li, and May Griffith. "Crosslinked collagen hydrogels as corneal implants: effects of sterically bulky vs. non-bulky carbodiimides as crosslinkers." *Acta biomaterialia* 9, no. 8 (2013): 7796-7805.

[9] Deng, Chao, Fengfu Li, Joanne M. Hackett, Shazia H. Chaudhry, Floyd N. Toll, Baldwin Toye, William Hodge, and May Griffith. "Collagen and glycopolymer based hydrogel for potential corneal application." *Acta biomaterialia* 6, no. 1 (2010): 187-194.

[10] Ahearne, Mark, and Amy P. Lynch. "Early observation of extracellular matrix-derived hydrogels for corneal stroma regeneration." *Tissue Engineering Part C: Methods* 21, no. 10 (2015): 1059-1069.

[11] Fernández-Pérez, Julia, and Mark Ahearne. "The impact of decellularization methods on extracellular matrix derived hydrogels." *Scientific reports* 9, no. 1 (2019): 1-12.

[12] Fernández-Pérez, Julia, Peter W. Madden, and Mark Ahearne. "Engineering a corneal stromal equivalent using a novel multi-layered fabrication assembly technique." *Tissue Engineering* ja (2020).

[13] Li, Xian, Xiaoxuan Ma, Daidi Fan, and Chenhui Zhu. "New suitable for tissue reconstruction injectable chitosan/collagen-based hydrogels." *Soft Matter* 8, no. 14 (2012): 3781-3790.

[14] Chitkara, Deepak, Ariella Shikanov, Neeraj Kumar, and Abraham J. Domb. "Biodegradable injectable in situ depot-forming drug delivery systems." *Macromolecular bioscience* 6, no. 12 (2006): 977-990.

[15] Shu, Xiao Zheng, Yanchun Liu, Fabio S. Palumbo, Yi Luo, and Glenn D. Prestwich. "In situ crosslinkable hyaluronan hydrogels for tissue engineering." *Biomaterials* 25, no. 7-8 (2004): 1339-1348.

[16] Elisseeff, J., K. Anseth, D. Sims, W. McIntosh, M. Randolph, and R. Langer. "Transdermal photopolymerization for minimally invasive implantation." *Proceedings of the National Academy of Sciences* 96, no. 6 (1999): 3104-3107.

[17] Cohen Addad, J. P., and Pierre-Gilles de Gennes. *Physical properties of polymeric gels*. 1996.

[18] Gao, Xuanyue, Yingshan Zhou, Guiping Ma, Suqing Shi, Dongzhi Yang, Fengmin Lu, and Jun Nie. "A water-soluble photocrosslinkable chitosan derivative prepared by Michael-addition reaction as a precursor for injectable hydrogel." *Carbohydrate polymers* 79, no. 3 (2010): 507-512.

[19] Drury, Jeanie L., and David J. Mooney. "Hydrogels for tissue engineering: scaffold design variables and applications." *Biomaterials* 24, no. 24 (2003): 4337-4351.

[20] Hu, Xiaobin. "Synthesis and properties of silk sericin-g-poly (acrylic acid-co-acrylamide) superabsorbent hydrogel." *Polymer Bulletin* 66, no. 4 (2011): 447-462.

[21] Kundu, Banani, and Subhas C. Kundu. "Silk sericin/polyacrylamide in situ forming hydrogels for dermal reconstruction." *Biomaterials* 33, no. 30 (2012): 7456-7467.

[22] Simons, Kai, and Stephen D. Fuller. "Cell surface polarity in epithelia." *Annual review of cell biology* 1, no. 1 (1985): 243-288.

[23] Tao, Hu, David L. Kaplan, and Fiorenzo G. Omenetto. "Silk materials–a road to sustainable high technology." *Advanced materials* 24, no. 21 (2012): 2824-2837.

[24] Ma, Dakun, Yansong Wang, and Wenjie Dai. "Silk fibroin-based biomaterials for musculoskeletal tissue engineering." *Materials Science and Engineering: C* 89 (2018): 456-469.

[25] Koh, Leng-Duei, Jingjie Yeo, Yeong Yuh Lee, Qunya Ong, Mingyong Han, and Benjamin CK Tee. "Advancing the frontiers of silk fibroin protein-based materials for futuristic electronics and clinical wound-healing (invited review)." *Materials Science and Engineering: C* 86 (2018): 151-172.

[26] Applegate, Matthew B., Benjamin P. Partlow, Jeannine Coburn, Benedetto Marelli, Christopher Pirie, Roberto Pineda, David L. Kaplan, and Fiorenzo G. Omenetto. "Photocrosslinking of silk fibroin using riboflavin for ocular prostheses." *Advanced materials* 28, no. 12 (2016): 2417-2420.

[27] Wang, Siran, Chiara E. Ghezzi, Rachel Gomes, Rachel E. Pollard, James L. Funderburgh, and David L. Kaplan. "In vitro 3D corneal tissue model with epithelium, stroma, and innervation." *Biomaterials* 112 (2017): 1-9.

[28] Lawrence, Brian D., Jeffrey K. Marchant, Mariya A. Pindrus, Fiorenzo G. Omenetto, and David L. Kaplan. "Silk film biomaterials for cornea tissue engineering." *Biomaterials* 30, no. 7 (2009): 1299-1308.

[29] Bray, Laura J., Karina A. George, S. Louise Ainscough, Dietmar W. Hutmacher, Traian V. Chirila, and Damien G. Harkin. "Human corneal epithelial equivalents constructed on Bombyx mori silk fibroin membranes." *Biomaterials* 32, no. 22 (2011): 5086-5091.

[30] Wu, Jian, Jelena Rnjak-Kovacina, Yiqin Du, Martha L. Funderburgh, David L. Kaplan, and James L. Funderburgh. "Corneal stromal bioequivalents secreted on patterned silk substrates." *Biomaterials* 35, no. 12 (2014): 3744-3755.

[31] Niu, Chunqing, Xiang Li, Yiyu Wang, Xinyu Liu, Jian Shi, and Xinyu Wang. "Design and performance of a poly (vinyl alcohol)/silk fibroin enzymatically crosslinked semi-interpenetrating hydrogel for a potential hydrophobic drug delivery." RSC advances 9, no. 70 (2019): 41074-41082.

[32] Mandal, Biman B., Sonia Kapoor, and Subhas C. Kundu. "Silk fibroin/polyacrylamide semi-interpenetrating network hydrogels for controlled drug release." Biomaterials 30, no. 14 (2009): 2826-2836.

[33] Kweon, HaeYong, Joo-hong Yeo, Kwang-gill Lee, Hyun Chul Lee, Hee Sam Na, Young Ho Won, and Chong Su Cho. "Semi-interpenetrating polymer networks composed of silk fibroin and poly (ethylene glycol) for wound dressing." Biomedical materials 3, no. 3 (2008): 034115.

[34] Chen, Qian, Yuanhao Sima, Zhihao Liu, Yang Wang, Lan Shen, Chaoqun Zhang, and Huichao Yan. "Preparation and Properties of Semi-Interpenetrating Silk Fibroin Protein Hydrogels with Integrated Strength and Toughness." ACS Applied Polymer Materials 4, no. 1 (2021): 735-745.

[35] Park, Hyojin, Kinam Park, and Dukjoon Kim. "Preparation and swelling behavior of chitosan-based superporous hydrogels for gastric retention application." *Journal of Biomedical Materials Research Part A: An Official Journal of The Society for Biomaterials, The Japanese Society for Biomaterials, and The Australian Society for Biomaterials and the Korean Society for Biomaterials* 76, no. 1 (2006): 144-150.

[36] Mequanint, Kibret, Alpesh Patel, and Deon Bezuidenhout. "Synthesis, swelling behavior, and biocompatibility of novel physically cross-linked polyurethane-b lock-poly (glycerol methacrylate) hydrogels." *Biomacromolecules* 7, no. 3 (2006): 883-891.

[37] Nilasaroya, Anastasia, Laura A. Poole-Warren, John M. Whitelock, and Penny Jo Martens. "Structural and functional characterisation of poly (vinyl alcohol) and heparin hydrogels." *Biomaterials* 29, no. 35 (2008): 4658-4664.

[38] Lynch, Amy P., Finbarr O'Sullivan, and Mark Ahearne. "The effect of growth factor supplementation on corneal stromal cell phenotype in vitro using a serum-free media." *Experimental eye research* 151 (2016): 26-37.

[39] Bhattacharjee, Promita, Julia Fernández-Pérez, and Mark Ahearne. "Potential for combined delivery of riboflavin and all-trans retinoic acid, from silk fibroin for corneal bioengineering." *Materials Science and Engineering: C* 105 (2019): 110093.

[40] Zhang, Youwei, Zhouxi Wang, Yansong Wang, Jiongxin Zhao, and Chengxun Wu. "Facile preparation of pH-responsive gelatin-based core–shell polymeric nanoparticles at high concentrations via template polymerization." *Polymer* 48, no. 19 (2007): 5639-5645.

[41] Rajvaidya, Sangita, R. Bajpai, and A. K. Bajpai. "Morphological, thermal and annealed microhardness characterization of gelatin based interpenetrating networks of polyacrylonitrile: A hard biopolymer." *Bulletin of Materials Science* 28, no. 6 (2005): 529-534.

[42] Schneider, M., C. Graillat, S. Boutti, and T. F. McKenna. "Decomposition of APS and H2O2 for emulsion polymerisation." *Polymer Bulletin* 47, no. 3-4 (2001): 269-275.

[43] Mohan, Y. Murali, and Kurt E. Geckeler. "Polyampholytic hydrogels: Poly (N-isopropylacrylamide)-based stimuli-responsive networks with poly (ethyleneimine)." *Reactive and Functional Polymers* 67, no. 2 (2007): 144-155.

[44] Tretinnikov, Oleg N., and Yasushi Tamada. "Influence of casting temperature on the near-surface structure and wettability of cast silk fibroin films." *Langmuir* 17, no. 23 (2001): 7406-7413.

[45] Nayak, B. R., and R. P. Singh. "Development of graft copolymer flocculating agents based on hydroxypropyl guar gum and acrylamide." *Journal of Applied Polymer Science* 81, no. 7 (2001): 1776-1785.

[46] Pan, Zhen, and Jiandong Ding. "Poly (lactide-co-glycolide) porous scaffolds for tissue engineering and regenerative medicine." *Interface focus* 2, no. 3 (2012): 366-377.

[47] Li, Mingzhong, Masayo Ogiso, and Norihiko Minoura. "Enzymatic degradation behavior of porous silk fibroin sheets." *Biomaterials* 24, no. 2 (2003): 357-365.

[48] Foster, James W., Ricardo M. Gouveia, and Che J. Connon. "Low-glucose enhances keratocyte-characteristic phenotype from corneal stromal cells in serum-free conditions." *Scientific reports* 5, no. 1 (2015): 1-16.

[49] Joseph, Annie, Parwez Hossain, Seema Jham, Rhodri E. Jones, Paddy Tighe, Richard S. McIntosh, and Harminder S. Dua. "Expression of CD34 and L-selectin on human corneal keratocytes." *Investigative ophthalmology & visual science* 44, no. 11 (2003): 4689-4692.

[50] Peng, Henry T., and Pang N. Shek. "Development of in situ-forming hydrogels for hemorrhage control." *Journal of Materials Science: Materials in Medicine* 20, no. 8 (2009): 1753-1762.

[51] Kang, Hye-Won, Yasuhiko Tabata, and Yoshito Ikada. "Fabrication of porous gelatin scaffolds for tissue engineering." *Biomaterials* 20, no. 14 (1999): 1339-1344.

[52] Tan, Qinggang, Songgang Li, Jie Ren, and Chu Chen. "Fabrication of porous scaffolds with a controllable microstructure and mechanical properties by porogen fusion technique." *International journal of molecular sciences* 12, no. 2 (2011): 890-904.

[53] Grenier, Jérôme, Hervé Duval, Fabrice Barou, Pin Lv, Bertrand David, and Didier Letourneur. "Mechanisms of pore formation in hydrogel scaffolds textured by freeze-drying." Acta biomaterialia 94 (2019): 195-203

[54] Annabi, Nasim, Jason W. Nichol, Xia Zhong, Chengdong Ji, Sandeep Koshy, Ali Khademhosseini, and Fariba Dehghani. "Controlling the porosity and microarchitecture of hydrogels for tissue engineering." Tissue Engineering Part B: Reviews 16, no. 4 (2010): 371-383.

[55] Whang, K., K. E. Healy, D. R. Elenz, E. K. Nam, D. C. Tsai, C. H. Thomas, G. W. Nuber, F. H. Glorieux, R. Travers, and S. M. Sprague. "Engineering bone regeneration with bioabsorbable scaffolds with novel microarchitecture." *Tissue engineering* 5, no. 1 (1999): 35-51.

[56] Lim, Jun Sik, Chang Seok Ki, Jong Wook Kim, Kwang Gil Lee, Seok Woo Kang, Hae Yong Kweon, and Young Hwan Park. "Fabrication and evaluation of poly (epsilon-caprolactone)/silk fibroin blend nanofibrous scaffold." *Biopolymers* 97, no. 5 (2012): 265-275.

[57] Aramwit, Pornanong, Tippawan Siritientong, Sorada Kanokpanont, and Teerapol Srichana. "Formulation and characterization of silk sericin–PVA scaffold crosslinked with genipin." *International Journal of Biological Macromolecules* 47, no. 5 (2010): 668-675.

[58] Shamsudeen, Rahna K., Shiny Nair, and V. G. Jayakumari. "Equilibrium swelling, conductivity and electroactive characteristics of polyacrylamide hydrogels." *Indian J Eng Mater Sci* 13,(2006):62-68.

[59] Shupe, Russell D. "Chemical stability of polyacrylamide polymers." Journal of Petroleum Technology 33, no. 08 (1981): 1513-1529

[60] Xiong, Boya, Rebeca Dettam Loss, Derrick Shields, Taylor Pawlik, Richard Hochreiter, Andrew L. Zydney, and Manish Kumar. "Polyacrylamide degradation and its implications in environmental systems." NPJ Clean Water 1, no. 1 (2018): 1-9.

[61] Kim, Sangjoon, Ganesh Iyer, Arunan Nadarajah, Jonathan M. Frantz, and Alison L. Spongberg. "Polyacrylamide hydrogel properties for horticultural applications." *International Journal of Polymer Analysis and Characterization* 15, no. 5 (2010): 307-318.

[62] Koo, Stephanie, Sang Joon Ahn, Hao Zhang, Jenn C. Wang, and Evelyn KF Yim. "Human corneal keratocyte response to micro-and nano-gratings on chitosan and PDMS." *Cellular and Molecular Bioengineering* 4, no. 3 (2011): 399.

[63] Qazi, Y., Wong, G., Monson, B., Stringham, J. and Ambati, B.K., 2010. Corneal transparency: genesis, maintenance and dysfunction. *Brain research bulletin*, *81*(2-3), pp.198-210.

[64] Jester, James V., Patricia A. Barry, Georgia J. Lind, W. Matthew Petroll, Randa Garana, and H. Dwight Cavanagh. "Corneal keratocytes: in situ and in vitro organization of cytoskeletal contractile proteins." *Investigative ophthalmology & visual science* 35, no. 2 (1994): 730-743.

## Figures and Tables

**Table 1:** Pore size, porosity (%) and sol fraction (%) of PA/SF hydrogels fabricated at varying SF concentrations ranges from 4 to 8 wt%. Sol fraction (%) of silk fibroin semi-interpenetrating structural networks at 37°C. Data are shown as mean ± standard deviation, n = 3

**Fig. 1:** The representation of the possible free-radical polymerization mechanism to develop PA/SF semi-interpenetrating network hydrogel

**Fig. 2:** Physical, optical and morphology analysis: (a) Gelation time of PA/SF composite hydrogels as a function of different silk fibroin concentration at room temperature. The total polymer concentration was 15 wt% while the protein concentration varies 4-8 wt%. (b) Viscosity assessments of fabricated hydrogels with increasing shear rates. (c) Light transmittance of as-fabricated hydrogels. (d) Scanning electron micrographs of lyophilized hydrogels with different SF concentration. Only PA hydrogel shows the smallest pores. With the incorporation of SF protein, regular interconnected porous structure was developed

**Fig. 3:** Chemical, thermal and protein release profile analysis:(a) Fourier transform infrared spectra of silk fibroin (SF) solution; polyacrylamide (PA); PA/SF cross-linked semi-interpenetrating network hydrogels (b) Thermal stability of the fabricated hydrogels (c) Cumulative release profiles of SF from the composite hydrogels at 37°C in PBS (pH 7.4).

**Fig. 4:** Bio-physical characterization:(a) Swelling ratio of PA/SF hydrogels in de-ionized water at 37° C over time as a function of SF concentration; (b) Equilibrium swelling ratio of composite hydrogels in PBS of different pH (3, 7.4 and 11) as a function of composition at 37° C. The degradation of hydrogels at 37 °C in (c) buffer solution (PBS, pH 7.4) or (d) Protease XIV solution. The extent of degradation was expressed in terms of weight remaining (%) at each time point.

**Fig. 5:** Biocompatibility studies:(a) Initial cell attachment proficiency (b) total cell metabolism (c) viability of corneal stromal cells on different fabricated hydrogels using live/dead assay (live cells appear green and dead cells appear red) imaged using confocal microscopy on day 5. (d) Cytoskeletal organization of corneal stromal cells after 10 days in culture after staining actin filaments (red) and nuclei (blue).

**Fig. 6:** Quantification of genes and extracellular matrix: (a) Fold change gene expression analysis of corneal keratocyte-specific markers KERA, ALDH3A1, DCN and LUM and extracellular matrix markers COL1A1, COL3A1, COL5A1 as quantified by rtPCR. Gene expression was normalized to GAPDH. (b) Combined sGAG production in hydrogel construct and culture media as quantified by DMMB assay and ratio of sGAG/DNA present after 7 and 14 days.

**Fig. 7:** Immunofluorescent staining of protein markers ALDH3A1, αSMA and CD-34 (all green) and nuclei (blue) after 14 days in culture. Scale bar = 100μm.

**Table 1:** Pore size, porosity (%) and sol fraction (%) of PA/SF hydrogels fabricated at varying SF concentrations ranges from 4 to 8 wt%. Sol fraction (%) of silk fibroin semi-interpenetrating structural networks at 37°C. Data are shown as mean ± standard deviation, n = 3

| **Hydrogels** | **PA** | **PA/SF4** | **PA/SF6** | **PA/SF8** |
|---|---|---|---|---|
| **Average pore size (µm)** | 26.24±3.7 | 66.3±6.2 | 52.1±6.3 | 32.36±7.4 |
| **Porosity (%)** | 79.25±8.51 | 83.92±10.63 | 84.27±9.87 | 83.24±9.56 |
| **Sol fraction (%)** | 0.634±0.53 | 2.203±1.05 | 3.573±0.97 | 5.896±1.08 |

Figure 1



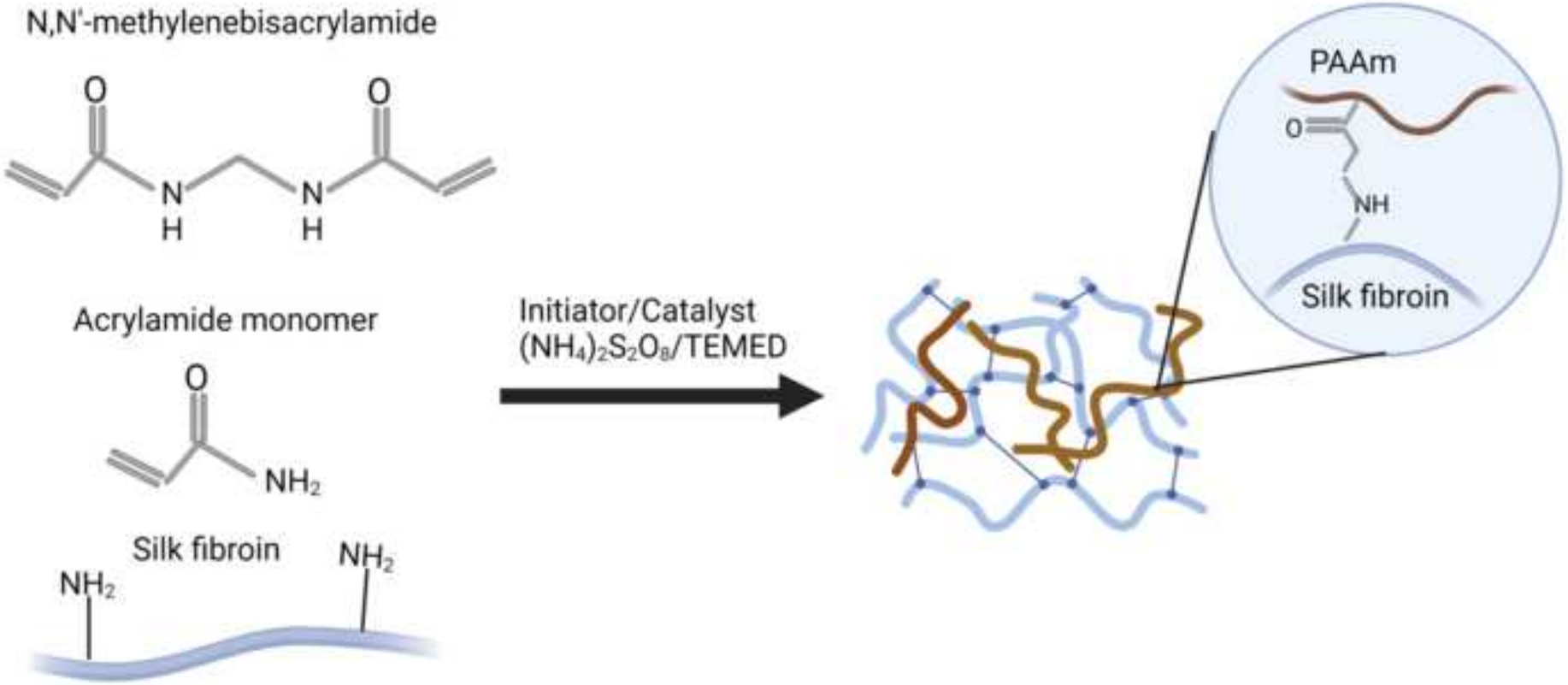

Figure 2

Click here to access/download;Figure;Figure 2.tif

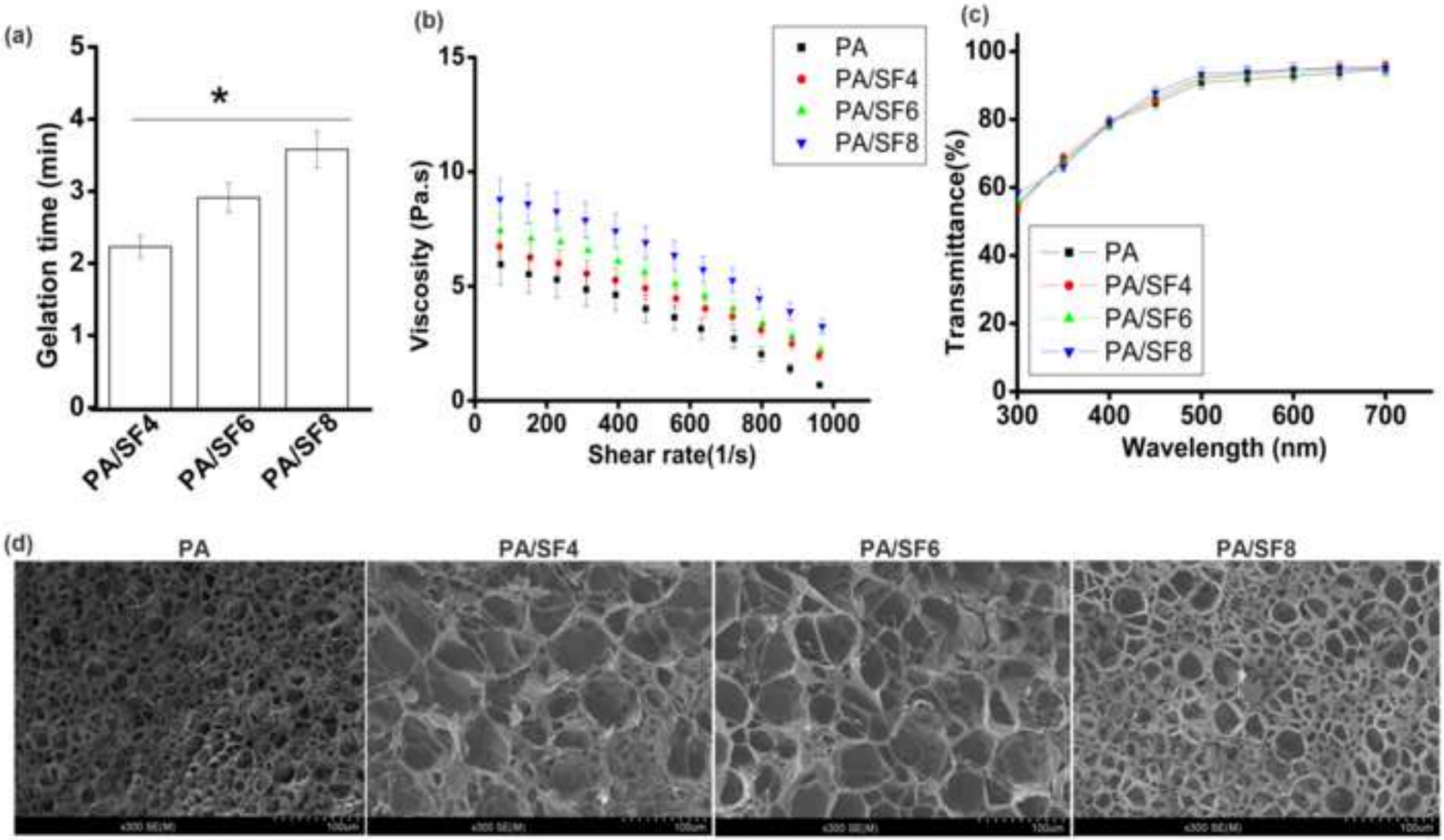

Figure 3

Click here to access/download;Figure;Figure 3.tif

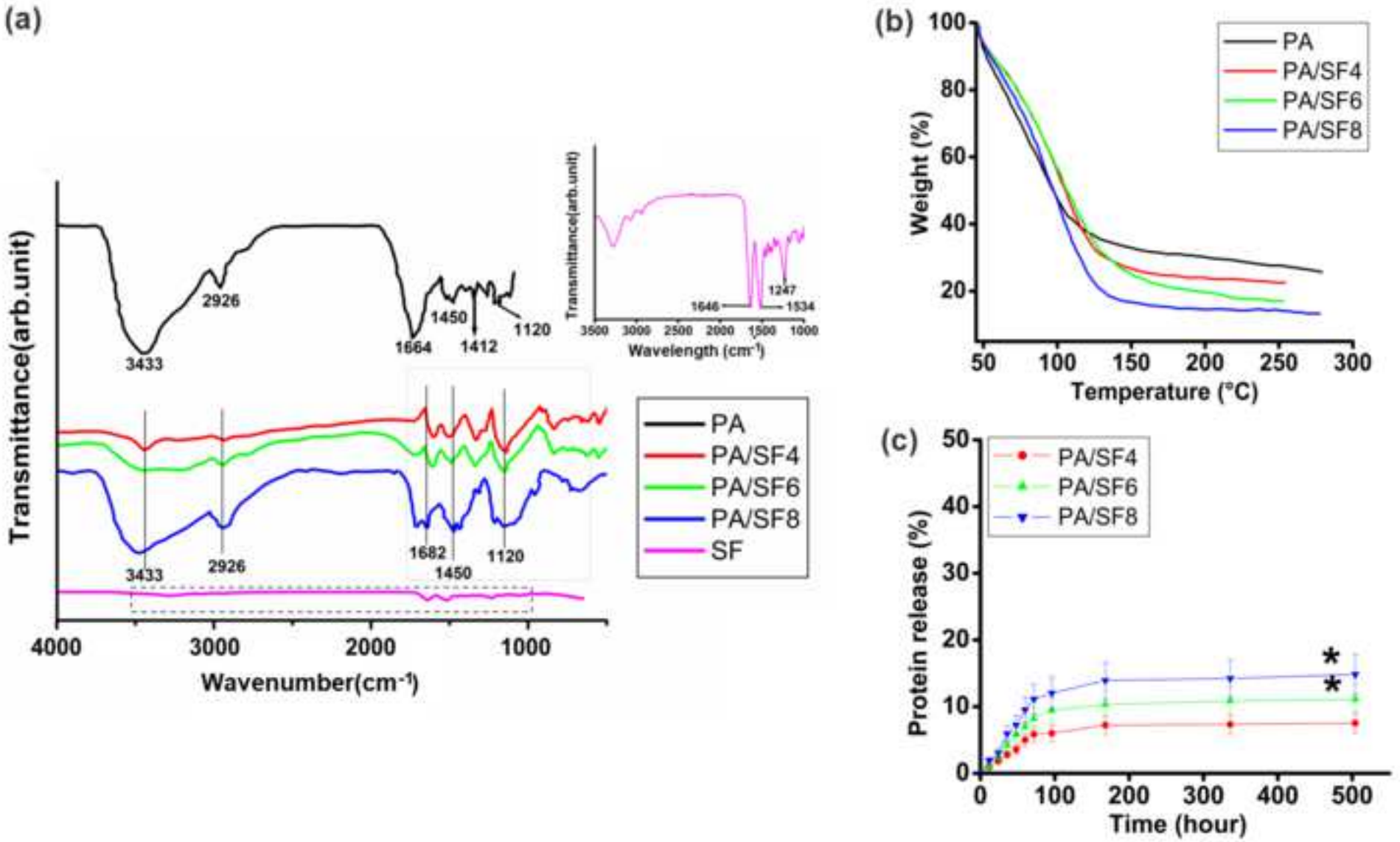

Figure 4

Click here to access/download;Figure;Figure 4.tif

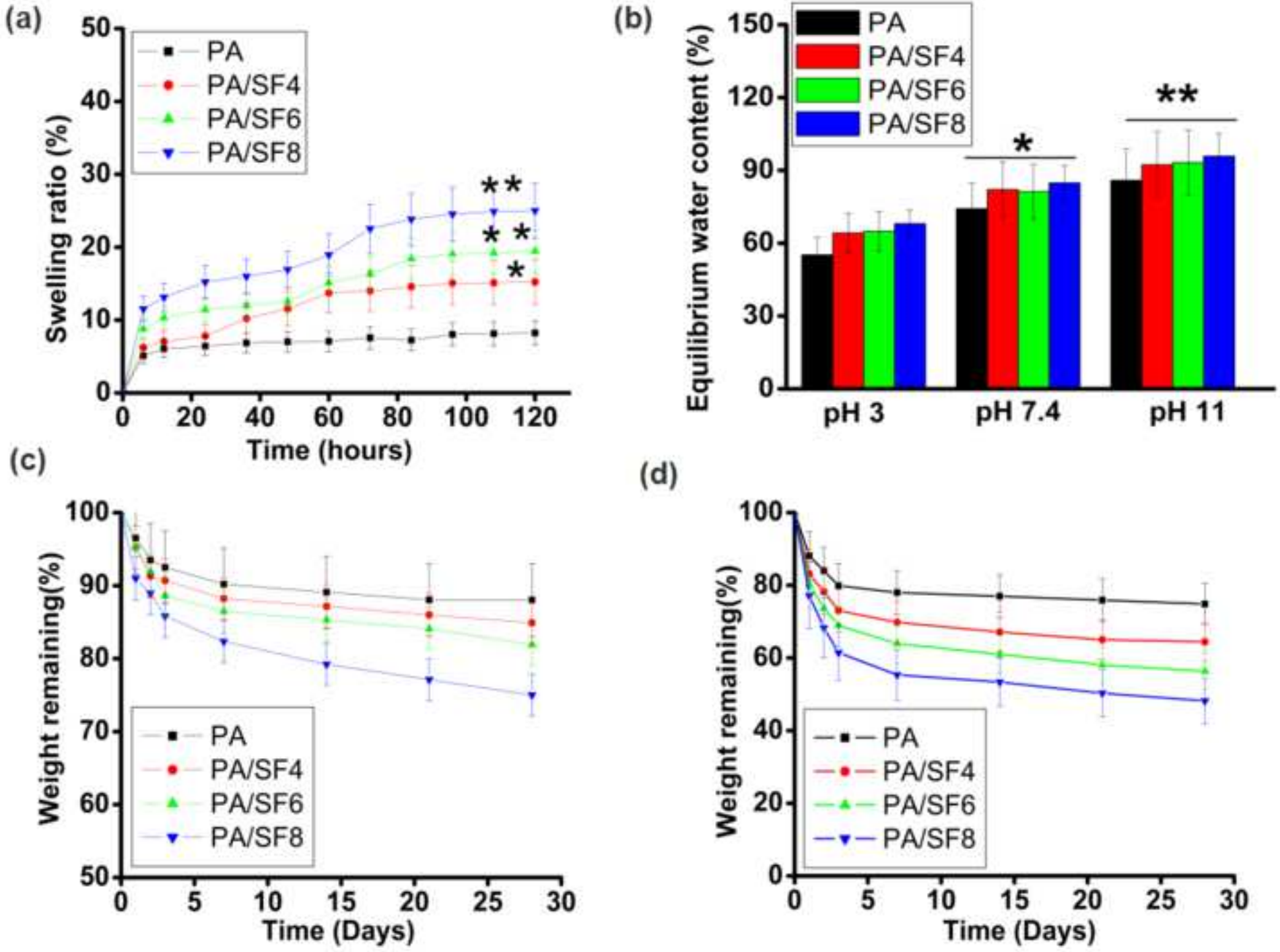

Figure 5

Click here to access/download;Figure;Figure 5.tif

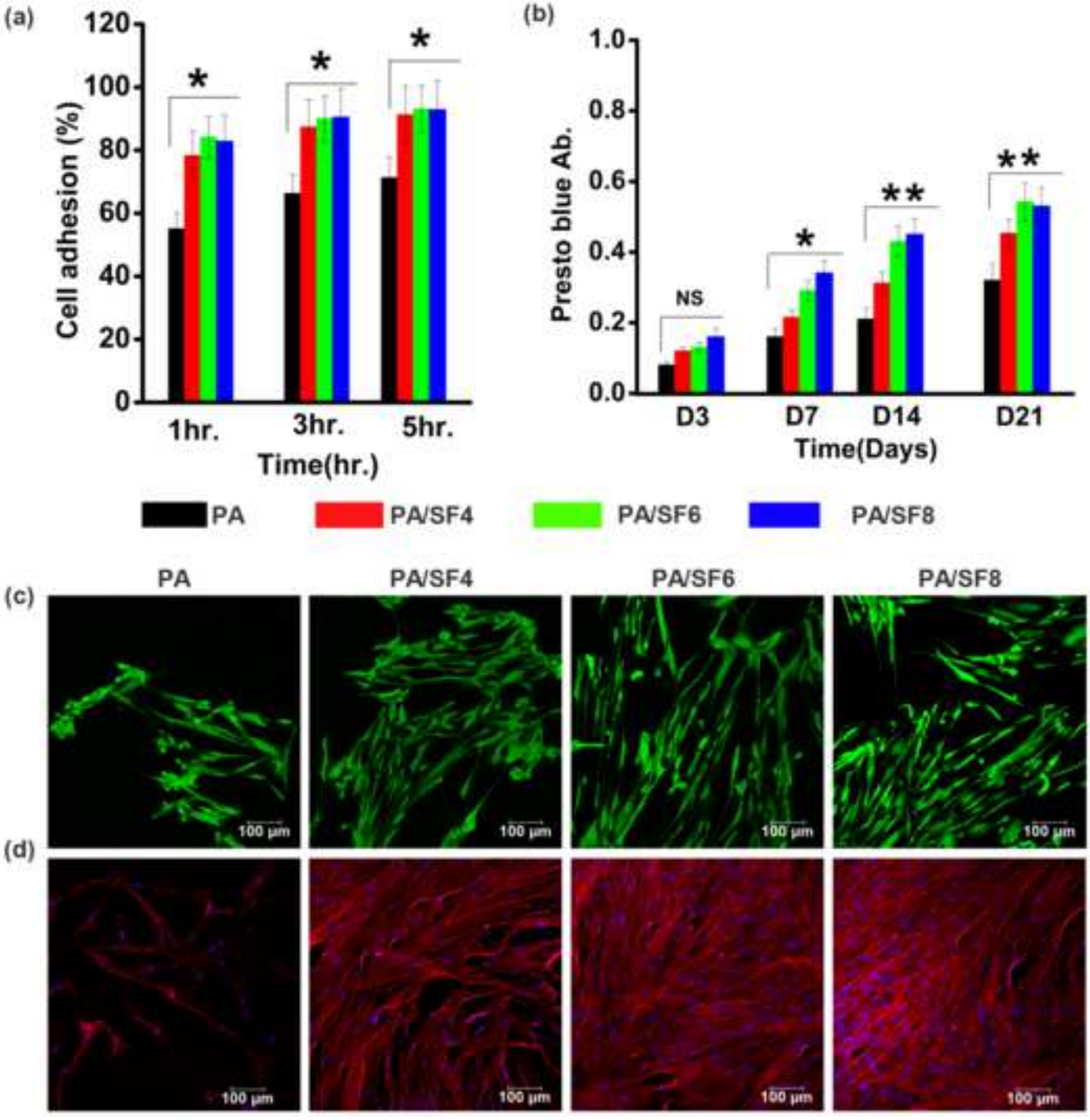

Figure 6



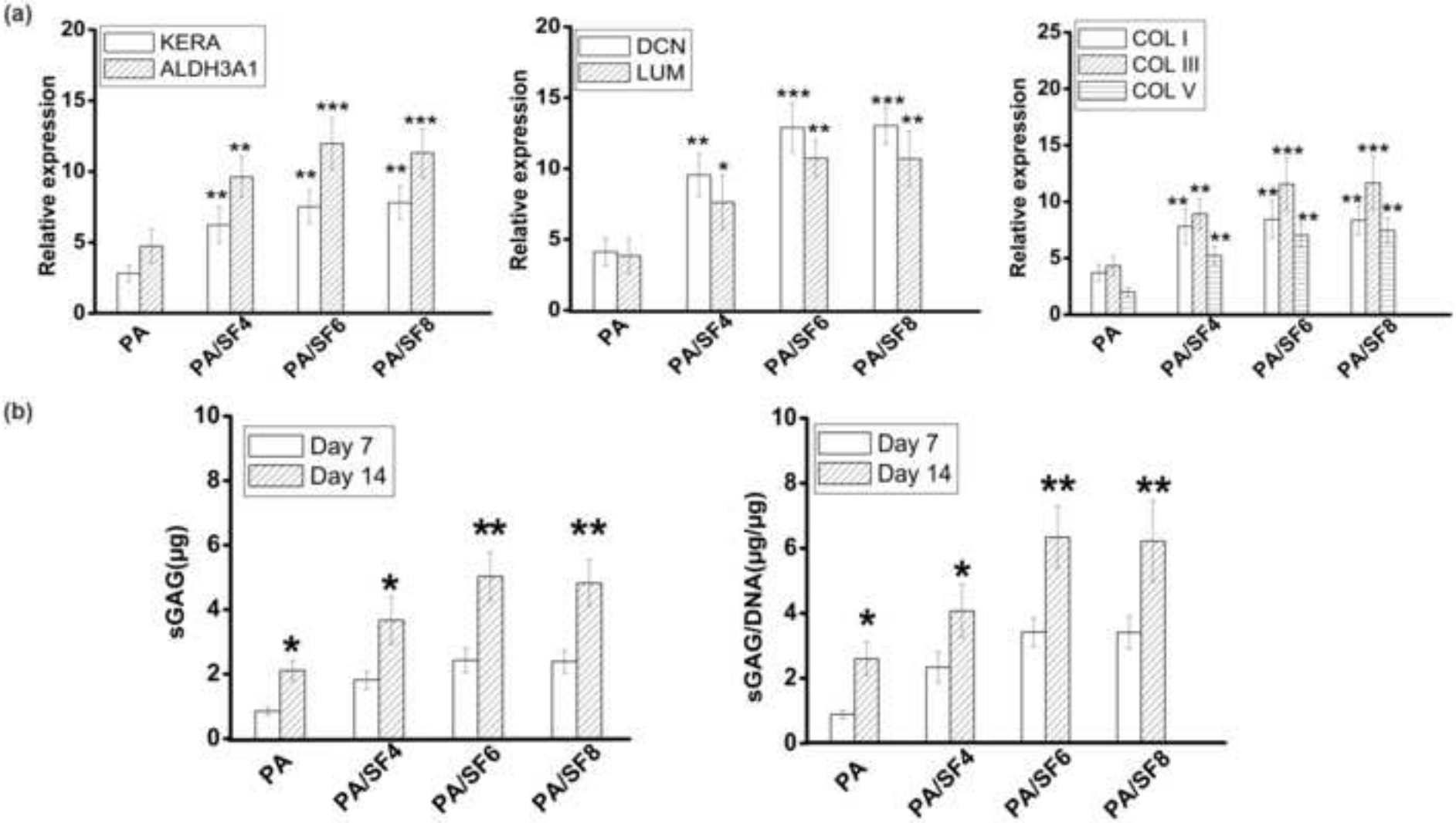

Figure 7

Click here to access/download;Figure;Figure 7.tif